Synthesis of $Ba_{1-x}Sr_xYSi_2O_5N$ and Discussion based on Structure Analysis and DFT Calculation

Takuya Yasunaga[a], Makoto Kobayashi[b,*], Kenta Hongo[c,d,e,f,g], Kotaro Fujii[h], Shunsuke Yamamoto[a], Ryo Maezono[f,g], Masatomo Yashima[h], Masaya Mitsuishi[a], Hideki Kato[a,*] and Masato Kakihana[a]

[a] Institute of Multidisciplinary Research for Advanced Materials, Tohoku University, 2-1-1 Katahira, Aoba-ku, Sendai, Miyagi 980-8577, Japan

[b] Institute of Materials and Systems for Sustainability, Nagoya University, Furo-cho, Chikusa-ku, Nagoya, Aichi 464-8601, Japan

[c] Research Center for Advanced Computing Infrastructure, Japan Advanced Institute of Science and Technology, Asahidai 1-1, Nomi, Ishikawa 923-1292, Japan

[d] Center for Materials Research by Information Integration, Research and Services Division of Materials Data and Integrated System, National Institute for Materials Science (NIMS), Tsukuba, Ibaraki 305-0047, Japan

[e] PRESTO, Japan Science and Technology Agency (JST), 4-1-8 Honcho, Kawaguchi-shi, Saitama 322-0012, Japan

[f] Computational Engineering Applications Unit, RIKEN, 2-1 Hirosawa, Wako, Saitama 351-0198, Japan

[g] School of Information Science, Japan Advanced Institute of Science and Technology, Asahidai 1-1, Nomi, Ishikawa 923-1292, Japan

[h] Department of Chemistry, School of Science, Tokyo Institute of Technology, 2-12-1-W4-17, O-okayama, Megro-ku, Tokyo 152-8551, Japan

* Corresponding authors: Makoto Kobayashi (mkoba@imass.nagoya-u.ac.jp)

Hideki Kato (hideki.kato.e2@tohoku.ac.jp)

Key words: Novel compound, Oxynitride, Phosphor, Computational chemistry

Abstract

Cation substitution for inorganic solid materials is a practical approach to control their functions. Here, synthesis, structure analysis, density functional theory (DFT) calculation of novel oxynitrides $Ba_{1-x}Sr_xYSi_2O_5N$, and investigation of their photoluminescence properties with Eu^{2+}- or Ce^{3+}-activator were conducted. Single crystal and powder X-ray analyses revealed that $Ba_{1-x}Sr_xYSi_2O_5N$ were formed at $x \leq 0.75$ and they were isotypic while the synthesis of $SrYSi_2O_5N$ ($x = 1$) was not achieved by any synthesis conditions examined. Based on phonon calculation, it was concluded that the synthesis of $SrYSi_2O_5N$ with the isostructure to $BaYSi_2O_5N$ was impossible due to the thermodynamical unstability. Substitution of Ba with Sr decreased the average bond length of *AE*-(O,N) (*AE* = Ba and Sr) and increased distortion of *AE* sites. On the other hand, coordination environments of Y sites were rarely affected by the substitution. As a result, redshift and broadening of emission spectra for Eu-doped samples were observed, whereas there was almost no spectral change in Ce-doped samples.

1. Introduction

In solid state chemistry, exploration of new compounds followed by synthesis of their derivatives including solid solutions is an important subject, because it often leads to high or new functional materials and extensive knowledge. With the development of computational chemistry such as materials informatics, a considerable amount of new compounds has been discovered, and the number of constituent elements in targeted compounds is increasing [1–5]. Under such circumstances, compounds with mixed anion are attractive targets because they show unique properties compared with conventional single anion materials such as oxides, nitrides, and fluorides [6]. The fact encourages many researchers to synthesize novel mixed anion compounds. As a result, mixed anion compounds having not only one or two but also three or more cations have been reported [7–12]. However, synthesis conditions should be precisely controlled to obtain such complicated compounds. It is, therefore, difficult to judge whether "this compound does not exist" or "this compound exists, however, the synthesis conditions are not proper" even when a target compound is not obtained.

Phonon calculation based on the first principle method gives us helpful information on whether the compound is thermodynamically stable or unstable; if imaginary phonon modes are detected, the compound cannot exist [13–19]. Stoffel *et al.* explained that the high-temperature phase of $BaCeO_3$ is not stable at room temperature by phonon densities of states (DOS) calculation. Schneider *et al.* have determined the crystal structure of a novel compound $Li_2Ca_3[N_2]_3$ among possible candidate models with the assistance of phonon DOS calculation although conventional techniques such as electron microscopy and diffractometry were not critical [15]. The approach can also be applied to mixed anion compounds, *e.g.,* determination of

a structure of $La_2Si_4N_6C$ by Hermus *et al*. Thus, we can judge the formation possibility of target compounds with the phonon calculation whether imaginary phonon modes are absent or not [19].

Recently, we have preliminarily reported a crystal structure of the first compound in BaO-Y_2O_3-SiO_2-Si_3N_4 system, $BaYSi_2O_5N$ [20]. Its luminescence properties with either Eu^{2+} or Ce^{3+} activator were also investigated because Eu^{2+}- or Ce^{3+}-doped oxynitrides are extensively studied with the aim at application to white light emitting diodes [21]. Their substituted forms involving solid solutions may be good candidates for the application because luminescence properties can be controlled by element substitution. In this research, we performed synthesis, density functional theory (DFT) calculation, and investigation of photoluminescence properties of Sr-substituted $BaYSi_2O_5N$ ($Ba_{1-x}Sr_xYSi_2O_5N$). Their formation possibilities are also discussed based on crystal structure analysis and phonon calculation.

2. Experiment

2.1 Synthesis

$Ba_{1-x}Sr_xYSi_2O_5N$ (x = 0, 0.1, 0.25, 0.33, 0.5, 0.75, and 1) were synthesized by a solid state reaction method. A stoichiometric amount of $BaCO_3$ (Kanto Chemical, 99.9%), $SrCO_3$ (Furuuchi Chemical, 99.9%), Y_2O_3 (Wako Pure Chemical, 99.99%), SiO_2 (Fuso Chemical, 99.999%), and Si_3N_4 (Kojundo Chemical, 99.9%) was ground in an agate mortar with ethanol. For Eu^{2+} or Ce^{3+}-doped samples, 2 mol% of alkaline-earth carbonates or Y_2O_3 were replaced with Eu_2O_3 (Kanto Chemical, 99.9%) or CeO_2 (Kanto Chemical, 99.5%), respectively. The mixture was put on a carbon sheet on an alumina boat and heated at 1573 K for 4 h under 100 ml min^{-1} of N_2 flow. Then, it was cooled to 1373 K at a rate of 25 K h^{-1} and to 1173 K at a rate of

50 K h^{-1}. Colorless plate-like crystals (Figure S1) were picked up from the products for analysis. Powder samples were prepared by grinding the sintered ones.

2.2 Characterization

Single crystals were analyzed by single crystal X-ray diffraction (single crystal XRD, Rigaku, R-AXIS RAPID II) using Mo *Kα* radiation. Data collection, raw data conversion, empirical corrections for absorption, and the merging of equivalent reflections were carried out using the RAPID-AUTO system [22]. All calculations were conducted using the WinGX software package [23]. Crystal structures were depicted by VESTA [24]. Cation compositions of every single crystal were confirmed by energy dispersive X-ray (EDX) spectrometry using a scanning electron microscope (Hitachi, SU1510) equipped with an EDX detector (Horiba, X-act). Crystallographic files in CIF format for $BaYSi_2O_5N$ (x = 0), $Ba_{0.9}Sr_{0.1}YSi_2O_5N$ (x = 0.1), $Ba_{0.67}Sr_{0.33}YSi_2O_5N$ (x = 0.33), $Ba_{0.5}Sr_{0.5}YSi_2O_5N$ (x = 0.5), and $Ba_{0.25}Sr_{0.75}YSi_2O_5N$ (x = 0.75) have been deposited with the Cambridge Crystallographic Data Centre (CCDC) as CCDC 1903159, CCDC 1903160, CCDC 1903161, and CCDC 1903162, and CCDC 1903163, respectively. The obtained powders were characterized by powder XRD analysis (Bruker AXS, D2 Phaser) and lattice parameters were refined by Le Bail method using the TOPAS 4.2 program (Bruker). Photoluminescence (PL) and corresponding excitation (PLE) spectra were recorded at room temperature using a fluorescence spectrometer (Hitachi, F-7100). The other fluorescence spectrometer (Jasco, FP-6500) was also used for thermal quenching and quantum efficiency analyses. Time-resolved luminescence lifetime measurements were performed using a single photon counting system. A Q-switched Nd:YAG laser (5 ns, 10 Hz, 355 nm) was used as the

excitation source. Luminescence decay data were obtained using a streak camera (Hamamatsu Photonics, KK streak camera system C4334).

2.3 Calculation

Electronic band structure calculation and phonon simulations were performed using a plane-wave based DFT package, CASTEP, implemented in BIOVIA Materials Studio [25]. The Perdew-Burke-Ernzerhof (PBE) generalized gradient approximation (GGA) functional [26] was employed for all the present simulations. Cutoff energies were 489.8 eV and 600.0 eV for the band structure and the phonon dispersion, respectively. Monkhorst-Pack *k*-point mesh was 2 × 2 × 1 for both calculations. All the ionic cores were replaced with ultrasoft pseudopotentials [27] for the band structure calculations. Lattice parameters and atomic positions were fully relaxed where the convergence criteria were carefully chosen as follows: total energy tolerance 2.0×10^{-5} eV/atom, maximum force tolerance 0.05 eV/Å, maximum stress component 0.1 GPa, maximum displacement 2.0×10^{-3} Å. For the phonon calculations, all ionic cores were replaced with norm conserving pseudopotentials [28]. Since we adopted different pseudopotentials for the band structure and the phonon simulations, the geometries were re-optimized with the same convergence criteria as those for the band structure calculations. Note that the ultrasoft calculations gave almost the same optimized geometries as the norm-conserving ones, their differences in the bond lengths and volumes being less than 0.1 and 0.4%, respectively.

3. Results and discussion

3.1 Synthesis of $Ba_{1-x}Sr_xYSi_2O_5N$

Figure 1(a) shows XRD patterns of $Ba_{1-x}Sr_xYSi_2O_5N$ synthesized at x = 0, 0.1, 0.33, 0.5, 0.75, and 1 and a calculated pattern of $BaYSi_2O_5N$ based on our previous work [20]. Samples synthesized at x = 0 and 0.1 contained only $BaYSi_2O_5N$ phase. At $0.33 \leq x \leq 0.75$, the target material was formed as the main phase even though unidentified peaks were observed. Peak positions of the target phase were monotonically shifted to higher angles with the increase of the Sr content. The variation of the cell volumes for $Ba_{1-x}Sr_xYSi_2O_5N$ refined by Le Bail method is shown in Figure 1(b). The volumes decreased linearly with the increasing Sr, indicating that substitution of Sr for Ba was achieved and the Sr content in $Ba_{1-x}Sr_xYSi_2O_5N$ powders can be controlled by the Ba/Sr ratio in starting materials at $x \leq 0.75$. On the other hand, at x = 1, the formation of the target phase was not observed, instead, only unidentified peaks, some of which appeared in samples at $x \leq 0.75$, were present. Indexing for the pattern was not successful, indicating that the sample was composed of more than two phases. Synthesis of a $SrYSi_2O_5N$ phase with isostructure to $BaYSi_2O_5N$ was not achieved in spite of several trials with different synthesis conditions such as heating temperature and time. Further investigation about what compounds were formed from the synthesis at x = 1 is in progress.

3.2 Crystal structures of $Ba_{1-x}Sr_xYSi_2O_5N$

EDX analysis of every single crystal indicated that the ratios of Ba:Sr:Y:Si were almost consistent with the stoichiometric ones of the target compositions taking errors and the matrix effect into consideration (Table S1). Elemental analysis and single crystal XRD of samples synthesized at x = 0, 0.1, 0.33, 0.5, and 0.75 revealed that the compounds are isotypic and belong to monoclinic system ($C2/c$) with compositions of $BaYSi_2O_5N$, $Ba_{0.9}Sr_{0.1}YSi_2O_5N$, $Ba_{0.67}Sr_{0.33}YSi_2O_5N$, $Ba_{0.5}Sr_{0.5}YSi_2O_5N$, and $Ba_{0.25}Sr_{0.75}YSi_2O_5N$, respectively. Thus, it was

confirmed that Sr-substituted $BaYSi_2O_5N$ up to 75% can be formed even though unidentified peaks were observed at powder XRD patterns of the samples synthesized at $x \geq 0.33$. Crystallographic parameters are summarized in Table 1. The lattice parameters and volumes decrease with the increase in x due to the smaller ionic size of Sr than that of Ba (Ba^{2+}: 1.52 Å, Sr^{2+}: 1.36 Å at ten coordination). In other words, Sr was not substituted for Y in the present oxynitrides as discussed later.

Figure 2 shows the crystal structures of $BaYSi_2O_5N$ and $Ba_{0.25}Sr_{0.75}YSi_2O_5N$ as representatives of the present compounds. Nine anions sites with 8*f* were identified. Although it is difficult to distinguish between oxygen and nitrogen by XRD analysis, their sites and occupancy are sometimes identified by single crystal XRD based on coordination numbers of anions and bond length to adjacent metal ions [7,8,31–34]. However, a splitting Si site as discussed later makes it impossible to judge precisely in the present compounds. Therefore, oxygen and nitrogen were put uniformly at all sites in O:N = 5:1 in the present analysis. There are two different sites for *AE* (= Ba and Sr) and Y, respectively. The coordination numbers for *AE* are 9 (*AE*1) and 10 (*AE*2), and those for Y are 6 (Y1) and 8 (Y2) (Table S2). Whereas refinement using models with Ba or Sr at the Y1 site was unstable, refinement of Ba or Sr occupancies at the Y2 site was converged properly with less than 1% occupancy. Although occupation of Ba^{2+} and Y^{3+} at the same site was reported in some papers [16,35], we concluded that disorder of *AE* and Y at the same site was not reasonable in the present compounds considering differences of the ionic size (Ba^{2+}: 1.42 Å, Sr^{2+}: 1.26 Å, Y^{3+}: 1.02 Å at eight coordination) and the valences. Si ions locate at three different sites, Si1, Si2, and Si3. Si3 was analyzed as a split site, Si3A and Si3B, because the refinement with Si ions at each middle position instead of the split sites results in heavy distortion of thermal ellipsoids around Si3 site.

Site occupancies of Si ion at Si3A and Si3B sites, *g*(Si, Si3A) and *g*(Si, Si3B), were refined to be almost equal (0.472(7) versus 0.528(7) at $x = 0$ and 0.502(12) versus 0.498(12) at $x = 0.75$). The split is explained by the overlap of four different Si–(O,N), resulting in the possible formation of isolated $Si_3(O,N)_9$ or $Si_6(O,N)_{18}$ as discussed in our previous report [20].

The *g*(Sr, *AE*1) and *g*(Sr, *AE*2) increased with an increase of x monotonically (Figure S2). Sr was preferentially substituted for Ba at *AE*2 site although it was expected that Sr of a smaller ion is more likely to occupy the *AE*1 site with lower coordination number [36–38]. Coordination environments of *AE* sites are depicted in Figure 3. *AE*2 site is surrounded by two (O,N)1 and two (O,N)5. These anions make a square plane space by two-fold rotation axis. Lengths of *AE*2–(O,N)1 and *AE*2–(O,N)5 are 2.683(4) Å and 2.655(5) Å at $x = 0$, respectively (Table S2). On the other hand, the shortest bond length at *AE*1 is 2.659(5) Å, and other eight bond lengths are longer than 2.78 Å. Therefore, owing to the narrower space formed by four anions, Sr is preferentially substituted for Ba at *AE*2 site. Such a "narrow space effect" was observed in other systems [39].

The *g*(Sr, *AE*1) and *g*(Sr, *AE*2) for sample at $x = 0.75$ were refined to be 0.6420(3) and 0.9659(7). If only Sr occupies *AE*2 site, *g*(Sr, *AE*1) is 0.625 at $x = 0.75$ considering that *AE*1 and *AE*2 are 8*f* and 4*e* sites, respectively. Refinement parameters obtained using the model with *g*(Sr, *AE*1) = 0.625 and *g*(Sr, *AE*2) = 1 were almost the same as those mentioned in Table 1 (Table S3). Therefore, Sr can fully occupy the *AE*2 site in $BaYSi_2O_5N$ while *g*(Sr, Ba1) > 0.625 may not be allowed, resulting in the impossible formation of $SrYSi_2O_5N$.

3.3 Phonon calculation for $BaYSi_2O_5N$ and $SrYSi_2O_5N$

For phonon calculation, proper models should be built. Because the present compounds have the split site (Si3) and anion disorder, huge supercells are required to express the crystal structures authentically. It is time-consuming and not realistic. To find the proper model, we performed phonon calculation for $BaYSi_2O_5N$, which can be synthesized, with various possible arrangements of Si3. Then, we determined one structure, in which all Si3 occupied only Si3A (Figure S3a) because other models gave negative phonon modes. The $SrYSi_2O_5N$ model was built by replacement of all Ba with Sr in $BaYSi_2O_5N$ (Figure S3b). Anion occupancies were decided based on the coordination numbers of Si and bond length, Si−(O,N) [7,8,31–34]. The results of geometry optimizations for $BaYSi_2O_5N$ and $SrYSi_2O_5N$ are shown in Table S4. Figure 4 shows the phonon dispersions of $BaYSi_2O_5N$ and $SrYSi_2O_5N$ in reciprocal space. No imaginary phonon mode appeared for the model at $x = 0$ while phonon dispersion of $x = 1$ showed imaginary components depicted in red. Therefore, $SrYSi_2O_5N$ is thermodynamically unstable, and it can be concluded that the formation of $SrYSi_2O_5N$ with isostructure to $BaYSi_2O_5N$ is impossible with ambient pressure condition at least.

3.4 Photoluminescence properties

Figures 5a and b show PLE and PL spectra of Eu^{2+}- and Ce^{3+}-doped $Ba_{1-x}Sr_xYSi_2O_5N$ (x = 0, 0.1, 0.33, 0.5, and 0.75) powders, respectively. XRD measurements indicated that Eu^{2+}- and Ce^{3+}-doping did not change phase purities (Figures S4 and S5). Eu^{2+}-doped $BaYSi_2O_5N$ exhibited broad blue emission with a peak at 459 nm under excitation at 250−450 nm. With the increase in x, the emission peaks were redshifted from 459 nm to 472 nm, and the spectra broadened. Emission spectra were decomposed into two components, component 1 (high energy) and 2 (low energy), as shown in Figure S6, and the luminescence decay curves followed a

biexponential function (Figure S7). These results are reasonable because Eu^{2+} would occupy two distinct sites, *AE*1 and *AE*2. In general, shorter average bond lengths of Eu^{2+}–(O,N) cause larger crystal field splitting, and it results in smaller 5*d*-4*f* emission energy. Therefore, it can be concluded that the component 1 and 2 are attributed to emission from Eu^{2+} at *AE*2 and *AE*1, respectively. The two components were redshifted and broadened by substitution of Ba with Sr. Figure 6 shows the changing rate of the average *AE*–(O,N) bond length and distortion index *D* of *AE* polyhedra in $Ba_{1-x}Sr_xYSi_2O_5N$. The following equation defines the *D* [40,41]:

$$D = \frac{1}{n}\sum_{i=1}^{n}\frac{|l_i - l_{av}|}{l_{av}} \quad (1)$$

where l_i is the distance from the center atom to the *i*th coordinating atom, l_{av} is the average bond length, and *n* is the coordination number. Thus, when the distortion of a polyhedron is large, the *D* value is large. With the increase in *x*, the average bond length became short, and the *D* became large at both *AE* sites. These structural changes agree with the changes in emission properties by the substitution of Ba with Sr, that is, redshift and broadening of spectra are attributed to bond length shortening and the *D* value increase by the substitution of Ba with Sr, respectively [42]. This relationship was also observed in other silicates such as Sr-substituted $Ba_3Si_6O_{12}N_2$ [32]. The samples synthesized at $x = 1$, which did not contain the target phase with the $BaYSi_2O_5N$ type structure, also exhibited PL, however, it was completely different from those of $Ba_{1-x}Y_xSi_2O_5N$. (Figure S8). Therefore, PL and PLE properties discussed above are independent of the phases giving unidentified peaks. Ce^{3+}-doped $BaYSi_2O_5N$ exhibited broad blue emission with a peak at 404 nm under excitation at 250−370 nm, and the peak positions of emission spectra were almost not affected by substitution of Ba with Sr. This is because the local structures of two kinds of Y sites, for which Ce is likely to be substituted, were not changed by the substitution of Ba with Sr.

External quantum efficiencies (EQE) of Eu^{2+} and Ce^{3+}-doped $BaYSi_2O_5N$ samples were 19.7% and 28.8%, respectively (Table S5, absorption rate and internal quantum efficiency are also summarized). The values decreased with the increase in x to 11.4% and 22.2%. This change may be attributed to the increase in the amount of impurities as discussed in the previous section (Figures S4 and S5). The PL intensity of the Eu-doped $BaYSi_2O_5N$ (x = 0) at 423 K was 32.5% of that at 298 K. The thermal quenching was suppressed by substitution of Ba with Sr, and 48.1% intensity to that at 298 K was observed for the sample at x = 0.75 (Figure S9a). Band gaps of x = 0 and 0.75 were calculated by DFT to be 2.53 and 3.14 eV, respectively (Figure S10). The large band gap of the host material prevents the photoionization of excited electrons, resulting in less thermal quenching [43,44]. Therefore, the band gap broadening by substitution of Ba with Sr contributed to less thermal quenching properties for Eu^{2+}-doped samples. On the other hand, the PL intensity of Ce-doped $BaYSi_2O_5N$ (x = 0) at 423 K was 52.7% of that at 298 K and the quenching property was not changed drastically by the substitution of Ba with Sr (56.9% at x = 0.75) (Figure S9b). Ce 5*d* level might be lower than that of Eu, resulting in that not photoionization but phonon-assisted relaxation dominantly influence the thermal quenching of the Ce-doped sample. [43,44].

4. Conclusion

$Ba_{1-x}Sr_xYSi_2O_5N$ solid solutions with an isotypic structure were successfully synthesized in the range of $0 \leq x \leq 0.75$, whereas formation of $SrYSi_2O_5N$ (x = 1) was not confirmed irrespective of synthesis conditions. Phonon calculation indicated that $SrYSi_2O_5N$ with the isostructure to the $BaYSi_2O_5N$ is unable to synthesize. Thus, the usefulness of the phonon calculation to judge the formation possibility of solid solutions has also been demonstrated in the

present system. The substitution of Ba with Sr changed local structures around alkaline earth metal sites and did not affect environments at yttrium sites. The substitution of Ba with Sr changed photoluminescence spectra and thermal quenching properties of Eu^{2+}-doped samples because local structures of alkaline earth metal sites and band gaps were altered. On the other hand, those properties for Ce^{3+}-doped samples were almost not affected by the substitution of Ba with Sr.

Acknowledgements

This work was supported in part by JSPS KAKENHI "Mixed anion" Grant Numbers JP16H06438, JP16H06439, JP16H06440, and 17H05478, and the Research Program of "Dynamic Alliance for Open Innovation Bridging Human, Environment and Materials". K. H. is grateful for financial support from a KAKENHI grant (JP17K17762) from MEXT, PRESTO (JPMJPR16NA) and the Materials research by the Information Integration Initiative (MI2I) project of the Support and Technology Agency (JST). R. M. is grateful for financial support from MEXT-KAKENHI (16KK0097), from Toyota Motor Corporation, from I-O DATA Foundation, and from the Air Force Office of Scientific Research (AFOSR-AOARD/ FA2386-17-1-4049). R. M. and K. H. are also grateful for financial support from MEXT-FLAGSHIP2020 (hp170269, hp170220).

Appendix A. Supplementary material

Supplementary data associated with this article can be found in the online version at doi:XXXX

References

[1] J. Greeley, T. F. Jaramillo, J. Bonde, I. Chorkendorff, J. K. Nørskov, Computational high-throughput screening of electrocatalytic materials for hydrogen evolution, *Nat. Mater.* 5 (2006) 909–913.

[2] G. Hautier, A. Jain, S. P. Ong, B. Kang, C. Moore, R. Doe, G. Ceder, Phosphates as lithium-ion battery cathodes: an evaluation based on high-throughput ab initio calculations, *Chem. Mater*. 23 (2011) 3495–3508.

[3] R. Gautier, X. Zhang, L. Hu, L. Yu, Y. Lin, T. O. L. Sunde, D. Chon, K. R. Poeppelmeier, A. Zunger, Prediction and accelerated laboratory discovery of previously unknown 18-electron ABX compounds, *Nat. Chem.* 7 (2015) 308–316.

[4] Z. Wang, J. Ha, Y. H. Kim, W. B. Im, J. McKittrick, S. P. Ong, Mining unexplored chemistries for phosphors for high-color-quality white-light-emitting diodes, *Joule* 2 (2018) 914–926.

[5] Y. Zhuo, A. M. Tehrani, A. O. Oliynyk, A. C. Duke, J. Brgoch, Identifying an efficient, thermally robust inorganic phosphor host via machine learning, *Nat. Commun.* 9 (2018) 4377–4386.

[6] H. Kageyama, K. Hayashi, K. Maeda, J. P. Attfield, Z. Hiroi, J. M. Rondinelli, K. R. Poeppelmeier, Expanding frontiers in materials chemistry and physics with multiple anions, *Nat, Commun.* 9 (2018) 772–786.

[7] D. Durach, L. Neudert, P. J. Schmidt, O. Oeckler, W. Schnick, $La_3BaSi_5N_9O_2:Ce^{3+}$ − a yellow phosphor with an unprecedented tetrahedra network structure investigated by

combination of electron microscopy and synchrotron X-ray diffraction, *Chem. Mater.* 27 (2015) 4832−4838.

[8] C. Maak, R. Niklaus, F. Friedrich, A. Mähringer, P. J. Schmidt, W. Schnick, Efficient yellow-orange phosphor $Lu_4Ba_2[Si_9ON_{16}]O:Eu^{2+}$ and orange-red emitting $Y_4Ba_2[Si_9ON_{16}]O:Eu^{2+}$: two oxonitridosilicate oxides with outstanding structural variety. *Chem. Mater.* 27 (2015) 4832−4838.

[9] W. B. Park, N. Shin, K.-P. Hong, M. Pyo, K.-S. Sohn, A New Paradigm for Materials Discovery: Heuristics-Assisted Combinatorial Chemistry Involving Parameterization of Material Novelty, *Adv. Funct. Mater.* 22 (2012) 2258–2266.

[10] W. B. Park, Y. S. Jeong, S. P. Singh, K.-S. Sohn, A Yellow-Emitting Oxynitride Phosphor: $Ce_{4-x}Ca_xSi_{12}O_{3+x}N_{18-x}:Eu^{2+}$, *ECS. J. Solid State Sci. Technol.* 2 (2013) R3100–R3106.

[11] W. Feldmann, P. L'Haridon, R. Marchand, Synthesis and Crystal Structure Determination of $Cs_3Mg_2P_6O_{17}N$: The First Example of a Nitrido-Oxo-Cyclohexaphosphate, *J. Solid State Chem.* 153 (2000) 185–191.

[12] A. Marchuk, L. Neudert, O. Oeckler, W. Schnick, $CaMg_2P_6O_3N_{10}$ – A Quinary Oxonitridophosphate with an Unprecedented Tetrahedra Network Structure Type, *Eur. J. Inorg. Chem.* 21 (2014) 3427–3434.

[13] R. P. Stoffel, C. Wessel, M. W. Lumey, R. Dronskowski, Ab initio thermochemistry of solid-state materials, *Angew. Chem. Int. Ed.* 49 (2010) 5242–5266.

[14] R. P. Stoffel, R. Dronskowski, First-principles investigations of the structural, vibrational and thermochemical properties of barium cerate – another test case for density-functional theory, *Z. Anorg. Allg. Chem.* 639 (2013) 1227–1231.

[15] S. B. Schneider, M. Seibald, V. L. Deringer, R. P. Stoffel, R. Frankovsky, G. M. Friederichs, H. Laqua, V. Duppel, G Jeschke, R. Dronskowski, W. Schnick, High-pressure synthesis and characterization of $Li_2Ca_3[N_2]_3$ -an uncommon metallic diazenide with $[N_2]^{2-}$ ions, *J. Am. Chem. Soc.* 135 (2013) 16668−16679.

[16] M. Hermus, P. C. Phan, J. Brgoch, Ab Initio Structure Determination and Photoluminescent Properties of an Efficient, Thermally Stable Blue Phosphor, $Ba_2Y_5B_5O_{17}:Ce^{3+}$, *Chem. Mater.* 28 (2016) 1121−1127.

[17] M. Hermus, A. M. Tehrani, J. Brgoch, Determining a structural distortion and anion ordering in $La_2Si_4N_6C$ via computation and experiment, *Inorg. Chem.* 55 (2016) 9454−9460.

[18] H. Y. Zhang, Z. Y. Zeng, Y. Q. Zhao, Q. Lu, Y. Cheng, First-principles study of lattice dynamics, structural phase transition, and thermodynamic properties of barium titanate, *Z. Naturforsch.* 71 (2016) 759–768.

[19] K. Nakano, H. Kenta, R. Maezono, Investigation into Structural Phase Transitions in Layered Titanium-Oxypnictides by a Computational Phonon Analysis, *Inorg. Chem.* 56 (2017) 13732-13740.

[20] M. Kobayashi, T. Yasunaga, H. Sato, H. Kato, K. Fujii, M. Yashima, M. Kakihana, Synthesis, structure, and photoluminescence of a novel oxynitride $BaYSi_2O_5N$ activated by Eu^{2+} and Ce^{3+}, *Chem. Lett.* 46 (2017) 795–797.

[21] L. Wang, R.-J. Xie, T. Suehiro, T. Takeda, N. Hirosaki, Down-Conversion Nitride Materials for Solid State Lighting: Recent Advances and Perspectives, *Chem. Rev.* 118 (2018) 1951–2009.

[22] RAPID-AUTO, Rigaku Corporation, Tokyo, Japan (2005).

[23] L. J. Farrugia, WinGX and ORTEP for Windows: an update, *J. Appl. Cryst.* 45 (2012) 849−854.

[24] K. Momma, F. Izumi, VESTA 3 for three-dimensional visualization of crystal, volumetric and morphology data, *J. Appl. Cryst.* 44 (2011) 1272–1276.

[25] S. J. Clark, M. D. Segall, C. J. Pickard, P. J. Hasnip, M. I. J. Probert, K. Refson, M. C. Payne, First principles methods using CASTEP, *Z. Kristallogr.* 220 (2005) 567–570.

[26] J. P. Perdew, K. Burke, M. Ernzerhof, Generalized Gradient Approximation Made Simple, *Phys. Rev. Lett.* 77 (1996) 3865–3868.

[27] D. Vanderbilt, Soft self-consistent pseudopotentials in a generalized eigenvalue formalism, *Phys. Rev. B*. 41 (1990) 7892–7895.

[28] D. H. Hamalm, M. Schluter, C. Chiang, Norm-Conserving Pseudopotentials, *Phys. Rev. Lett.* 43 (1979) 1494–1497.

[29] G. M. Sheldrick, SHELXT - Integrated space-group and crystal-structure determination, *Acta Cryst. A.* 71 (2015) 3−8.

[30] T. Higashi, *ABSCOR*, Rigaku Corporation, Tokyo, Japan (2001).

[31] H. A. Höppe, F. Stadler, O. Oeckler, W. Schnick, $Ca[Si_2O_2N_2]$—A Novel Layer Silicate, *Angew. Chem. Int. Ed.* 43 (2004) 5540 –5542.

[32] C. Braun, M. Seibald, S. L. Börger, O. Oeckler, D. T. Boyko, A. Moewes, G. Miehe, A. Tücks, W. W. Schnick, Material properties and structural characterization of $M_3Si_6O_{12}N_2:Eu^{2+}$ (M=Ba, Sr)—a comprehensive study on a promising green phosphor for pc-LEDs, *Chem. Eur. J.* 16 (2010) 9646–9657.

[33] X. M. Wang, C. H. Wang, M. M. Wu, Y. X. Wanga, X. P. Jing, O/N ordering in the structure of $Ca_3Si_2O_4N_2$ and the luminescence properties of the Ce^{3+} doped material, *J. Mater. Chem.* 22 (2012) 3388–3394.

[34] P. Strobel, D. T. Boer, V. Weiler, P. J. Schmidt, A. Moewes, W. Schnick, Luminescence of an oxonitridoberyllate: a study of narrow-band cyan-emitting $Sr[Be_6ON_4]:Eu^{2+}$, *Chem. Mater.* 30 (2018) 3122–3130.

[35] K. A. Denault, Z. Cheng, J. Brgoch, S. P. DenBaars, R. Seshadri, Structure–composition relationships and optical properties in cerium-substituted $(Sr,Ba)_3(Y,La)(BO_3)_3$ borate phosphors, *J. Mater. Chem. C.* 1 (2013) 7339–7345.

[36] Y. Sato, H. Kuwahara, H. Kato, M. Kobayashi, T. Masaki, M. Kakihana, Large Redshifts in Emission and Excitation from Eu^{2+}-Activated Sr_2SiO_4 and Ba_2SiO_4 Phosphors Induced by Controlling Eu^{2+} Occupancy on the Basis on Crystal-Site Engineering, *Opt. Photonics J.* 5 (2015) 326–333.

[37] Y. Sato, H. Kato, M. Kobayashi, T. Masaki, D.-H. Yoon, M. Kakihana, Tailoring of Deep‐Red Luminescence in $Ca_2SiO_4:Eu^{2+}$, *Angew. Chem., Int. Ed.*, 53 (2014) 7756–7759.

[38] D. Wen, H. Kuwahara, H. Kato, M. Kobayashi, Y. Sato, T. Masaki, M. Kakihana, Anomalous Orange Light-Emitting $(Sr,Ba)_2SiO_4:Eu^{2+}$ Phosphors for Warm White LEDs, *ACS Appl. Mater. Interfaces* 8 (2016) 11615–11620.

[39] D. Wen, H. Kato, M. Kobayashi, S. Yamamoto, M. Mitsuishi, M. Kakihana, Site occupancy and luminescence properties of $Ca_3Ln(AlO)_3(BO_3)_4:Ce^{3+},Tb^{3+},Mn^{2+}$ (Ln = Y, Gd), *J. Mater. Chem. C*. 5 (2017) 4578–4583.

[40] Z. Wang, W. Ye, I. H. Chu, S. P. Ong, Elucidating Structure−Composition−Property Relationships of the β-$SiAlON:Eu^{2+}$ Phosphor, *Chem. Mater.* 28(2016) 8622−8630.

[41] W. H. Baur, The Geometry of Polyhedral Distortions. Predictive Relationships for the Phosphate Group, *Acta Cryst.* B30 (1974) 1195–1215.

[42] Z. Wang, I. H. Chu, F. Zhou, S. P. Ong, Electronic Structure Descriptor for the Discovery of Narrow-Band Red-Emitting Phosphors, *Chem. Mater.* 28 (2016) 4024−4031.

[43] G. Blasse, Thermal Quenching of Characteristic Fluorescence, *J. Chem. Phys.* 51 (1969) 3529−3530.

[44] P. Dorenbos, Thermal quenching of Eu^{2+} 5*d*−4*f* luminescence in inorganic compounds. *J. Phys.: Condens. Matter.* 17 (2005) 8103–8111.

Table 1. Crystallographic parameters.

Formula	$BaYSi_2O_5N$	$Ba_{0.9}Sr_{0.1}YSi_2O_5N$	$Ba_{0.67}Sr_{0.33}YSi_2O_5N$	$Ba_{0.50}Sr_{0.50}YSi_2O_5N$	$Ba_{0.25}Sr_{0.75}YSi_2O_5N$
Crystal size / mm	0.040 × 0.037 × 0.030	0.050 × 0.030 × 0.030	0.055 × 0.030 × 0.015	0.050 × 0.050 × 0.025	0.040 × 0.040 × 0.015
Scan mode			ω scan		
Method of structure solution			Direct method, SHELXT [29]		
Type of absorption corrections			Multi-scan, *ABSCOR* [30]		
Crystal system, space group			Monoclinic, $C2/c$		
Lattice parameters					
a / Å	8.4655(3)	8.4568(2)	8.4284(4)	8.4064(4)	8.3671(4)
b / Å	10.2752(3)	10.2727(3)	10.2724(6)	10.2945(3)	10.2477(6)
c / Å	18.8146(8)	18.7959(4)	18.7445(9)	18.7279(6)	18.6150(11)
β / º	100.6420(10)	100.6000(10)	100.5550(10)	100.4890(10)	100.302(2)
V / Å^3	1608.43(10)	1605.01(7)	1595.43(14)	1593.62(10)	1570.38(15)
Formula units / cell			12		
Calculated density / gcm^{-1}	4.664	4.612	4.495	4.396	4.303
T / K	296(2)	298(2)	296(2)	296(2)	296(2)
Radiation			Mo $K\alpha$ (λ = 0.71073 Å)		
μ / mm^{-1}	18.467	18.772	19.507	19.975	20.949
No of measured, independent and observed [$I > 2\sigma(I)$] reflections	7558, 1826, 1689	7642, 1837, 1758	7674, 1829, 1711	7599, 1834, 1659	7479, 1796, 1603
T_{min}, T_{max}	0.525, 0.607	0.454, 0.603	0.413, 0.758	0.435, 0.635	0.488, 0.744
R_{int}	0.0382	0.0344	0.0338	0.0623	0.0599
$2\theta_{max}$	27.437	27.451	27.443	27.478	27.441
No. of reflections	1826	1837	1829	1834	1796
No. of parameters	148	150	150	150	1603
No. of restrains	0	0	0	0	0
GoF	1.104	1.038	1.144	1.096	1.257
R, wR [$F^2 > 2\sigma(F^2)$]	2.91%, 7.39%	2.31%, 5.60%	2.52%, 6.05%	3.56%, 9.12%	4.63%, 10.58%
R, wR (F^2)	3.26%, 7.52%	2.46%, 5.86%	2.78%, 6.18%	3.98%, 9.61%	5.18%, 10.82%
Min./ max. residual electron density / eÅ^{-3}	1.522, -1.928	1.038, -0.912	0.856, -1.097	1.360, -1.657	1.128, -1.237

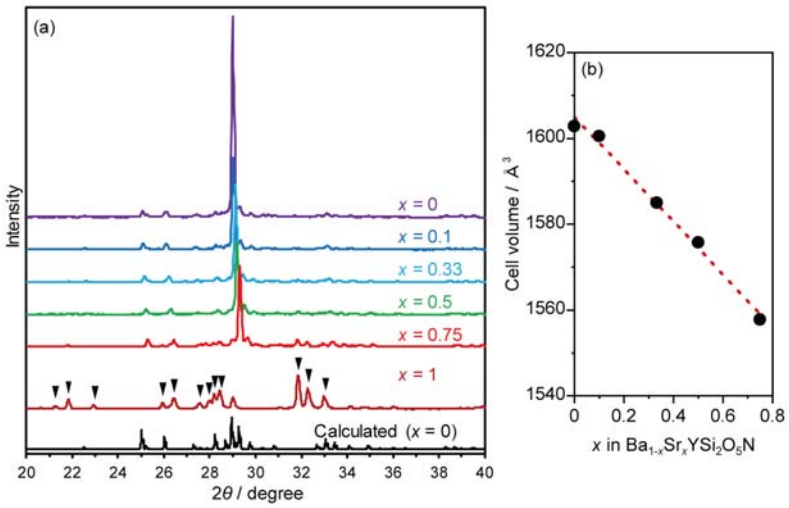

Figure 1. XRD patterns of $Ba_{1-x}Sr_xYSi_2O_5N$ samples synthesized at x = 0, 0.1, 0.33, 0.5, 0.75, and 1. (b) Cell volumes of $Ba_{1-x}Sr_xYSi_2O_5N$ powders.

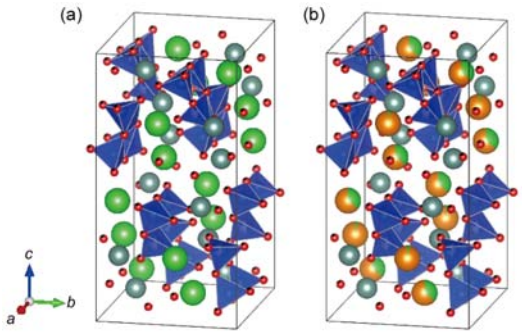

Figure 2. Crystal structures of (a) x = 0 and (b) x = 0.75 drawn with Ba (green), Sr (orange), Y (gray), Si (blue), O (red), N (black), and $Si(O,N)_4$ tetrahedra.

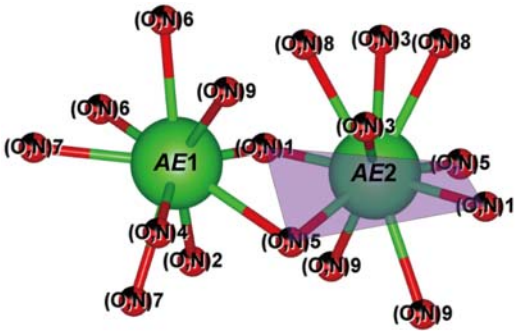

Figure 3. Coordination environments of *AE*1 and *AE*2 sites in $BaYSi_2O_5N$.

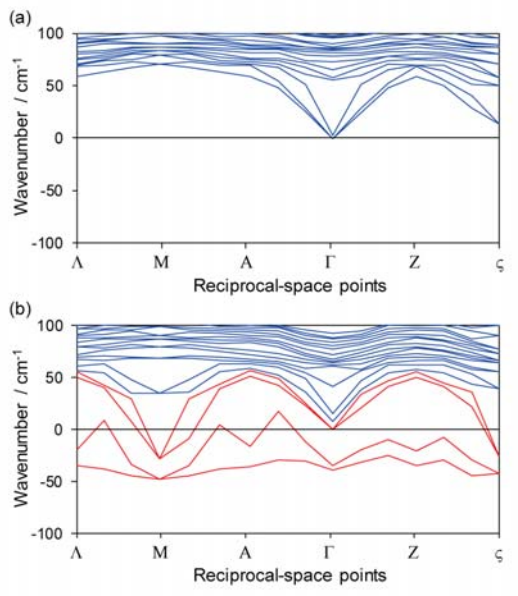

Figure 4. Phonon dispersions of (a) $x = 0$ and (b) $x = 1$.

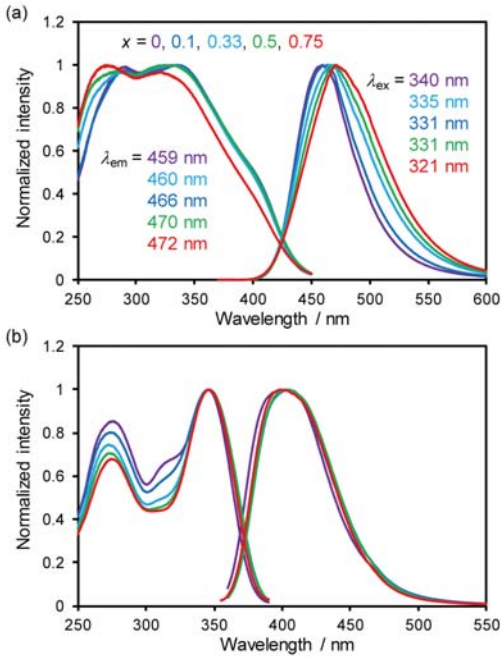

Figure 5. PL and PLE spectra of $Ba_{1-x}SrYSi_2O_5N$ (x = 0, 0.1, 0.33, 0.5, and 0.75) with 2 mol% (a) Eu- and (b) Ce-activators.

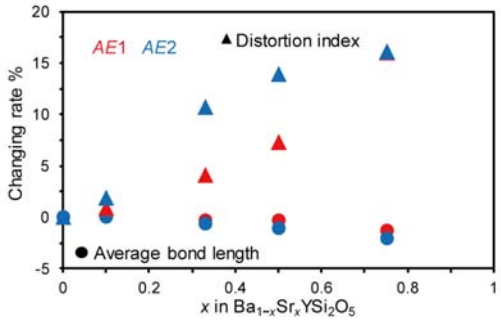

Figure 6. The changing rate of the average bond length to anions and distortion index of *AE*.